ELSEVIER

Contents lists available at ScienceDirect

Journal of Fluids and Structures

journal homepage: www.elsevier.com/locate/jfs



Bistability in the wake of a circular cylinder with passive control using two leeward rods



M.M. Cicolin a,b,*, P.W. Bearman a, G.R.S. Assi b, O.R.H. Buxton a

- ^a Department of Aeronautics, Imperial College London, SW7 2AZ, UK
- ^b Escola Politécnica, University of São Paulo, Brazil

ARTICLE INFO

Article history: Received 5 January 2023 Received in revised form 28 March 2023 Accepted 30 May 2023 Available online 16 June 2023

Keywords:
Fluid dynamics
Flow around bluff bodies
Control of flow
Coandă effect

ABSTRACT

This paper presents an experimental investigation on the flow around a circular cylinder controlled by a pair of rods placed close to the separated shear layers from the leeward face of the cylinder. Past research of Cicolin et al. (2021) has shown that one control rod, placed at specific positions, induces a late flow separation on the main cylinder's surface in a typical occurrence of the Coandă effect. As a result the control rod reduced the mean drag acting on the cylinder but also produced a net mean lift force. We now present an extension of the aforementioned study to consideration of a pair of symmetrically arranged control rods, aimed at eliminating the mean lift force whilst maintaining a drag reduction. The experiments were carried out at a Reynolds number Re = 20,000 based on the diameter of the main cylinder D, with the diameter of the control rods being ten times smaller than that of the cylinder. The centre-to-centre distances between each control rod and the cylinder was 0.7D, and the angular position of the rods varied from $\theta = 120^{\circ}$ to 125° , where θ is measured from the front stagnation point. Time-resolved PIV velocity fields and hydrodynamic forces were measured for the different setups. Results show that the mean flow is asymmetric in spite of the symmetry of the geometric model and position of the rods. The pair of control rods induces a bistable flow, induced by the imbalance of two colliding jets in the near wake. The dynamics were found to be random, with the average switching time between stable states depending on the position of the rods. The mean drag force was reduced by up to 15%, and the mean lift force was reduced by 80% compared to the cases with a single control rod. It was also observed that the control rod can induce two different types of flow separation from the main cylinder, one in which the flow separates from the main cylinder only once and one in which a small separation bubble forms in proximity to the control rod before reattaching and then permanently separating. These distinct features play an important role in the dynamics of the bistability and hint at a possible extension of the total drag reduction to 30% if the bistability is suppressed.

© 2023 The Authors. Published by Elsevier Ltd. This is an open access article under the CC BY license (http://creativecommons.org/licenses/by/4.0/).

1. Introduction

The flow past bluff bodies is an important area in fluid mechanics research, due to its prevalence in nature and in many engineering processes. Such flows are mainly characterised by a separated flow, the formation of a low pressure region in the near wake, and a vortex street (Bearman, 1984; Williamson, 1996). Their nature is more complex than flows past streamlined bodies and engenders several engineering challenges, e.g. flow-induced vibrations and noise (Blevins, 2001).

^{*} Corresponding author at: Department of Aeronautics, Imperial College London, SW7 2AZ, UK. E-mail addresses: mmcicolin@gmail.com, mm9116@ic.ac.uk (M.M. Cicolin).

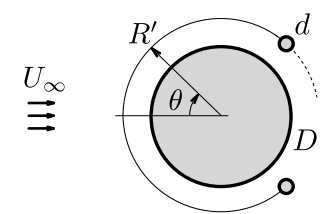


Fig. 1. Coordinate system and configuration for the cylinder-two-control-rods system. Note that *D* is the diameter of the main cylinder and *d* is the diameter of the control rod.

Bluff bodies have a larger drag coefficient than streamlined bodies. Additionally, flow-induced unsteady forces have a significant impact on the structural behaviour of bluff bodies and are particularly harmful when the body is allowed to oscillate freely (Williamson and Govardhan, 2004; Faltinsen, 1990). For example, the sea current around offshore structures such as riser pipes induces vortex-induced vibration that can lead the structure to fail by fatigue. Static structures like chimneys, bridges, and other civil structures are also affected by the wind, requiring an extra cost for resisting the aerodynamic forces (Païdoussis et al., 2010).

Whilst the bluff geometry of a particular body is the primary cause for the high hydrodynamic/aerodynamic forces acting on it, in many applications there is limited scope for hydrodynamic/aerodynamic optimisation due to geometric constraints imposed by other considerations, such as manufacturability or cost. For example, the circular cylinder is the most practical shape for many structures exposed to a flow (e.g. offshore risers), regardless of its poor hydrodynamic performance. Accordingly, improvement to hydrodynamic performance is sought via flow-control techniques, often using external devices. Choi et al. (2008) provides a comprehensive review of control methods for the flow past circular cylinders, and classifies the devices according to the type of actuator (passive or active methods), according to the region of actuation in the flow (boundary layer, shear layer, near wake etc.), and according to the forcing distribution characteristics along the span (2D versus 3D forcing). Active devices are more efficient in theory, but are highly sensitive to fluctuations of the incoming flow/control function and they are also typically more expensive. As a result, passive control methods are more commonly employed due to their simplicity, feasibility, and lower operational costs. They have been studied from both a theoretical and technological standpoint in the past few decades (Choi et al., 2008; Zdravkovich, 1981), and there is a continuous stream of research for novel solutions, as well as improvement and optimisation of known devices.

Control rods, also known as control cylinders, placed in close proximity to the main cylinder are one of the most common strategies for manipulating the flow past a cylinder. They are typical 2D forcing devices that rely on the idea that a small body can fundamentally change the wake development of the combined system (cylinder plus control rod/rods) by manipulating the separation and evolution of the shear layers emanating from the main cylinder and the subsequent interaction between the various separated shear layers within the system's wake. The arrangement of a pair of control rods, of diameter d, in proximity to a larger cylinder of diameter D is illustrated in Fig. 1. The use of a control rod to suppress the vortex shedding, and hence fluctuating force, over a circular cylinder was pioneered by the study of Strykowski and Sreenivasan (1990), which observed a complete suppression of vortex shedding by placing a small control rod in several positions across the wake. Their research was limited to a very low range of Reynolds numbers (Re) but it has motivated further studies varying different properties of the cylinder-control rod(s) system, illustrated in Fig. 1. These include Re, control-rod position $(R'/D, \theta)$, size (d/D) and number of rods, and also the shape of the main cylinder (Sakamoto and Haniu, 1994; Dalton et al., 2001; Yildirim et al., 2010; Tsutsui et al., 1997; Mittal and Raghuvanshi, 2001; Kuo et al., 2007; Bingham et al., 2018; Cicolin et al., 2021; Assi et al., 2019; Sakamoto et al., 1991; Parezanovic and Cadot, 2012; Parezanovic et al., 2015; Chauhan et al., 2019). A summary of past studies on control rods, varying these parameters, can be found in the introduction of Cicolin et al. (2021). More recently, some researchers have investigated the effectiveness of control rods to suppress vortex-induced vibration (Zhu et al., 2015; Jimenez-Gonzalez and Huera-Huarte, 2017; Jiménez-González and Huera-Huarte, 2018; Assi et al., 2019).

All the works cited above show a condition in which the mean drag force is reduced, and the fluctuating lift suppressed or attenuated. However, the optimal placement of the control rod(s) varied significantly across the various studies. This is primarily due to the high sensitivity of the wake to the exact positioning of the control rod(s) yielding fundamentally different flow states as the control rod(s) position is varied (Cicolin et al., 2021). Some examples of the different flow states identified by Cicolin et al. (2021) are illustrated in Fig. 2. Sakamoto and Haniu (1994), Cicolin et al. (2021), Parezanovic and Cadot (2012), Bingham et al. (2018) showed that the wake can develop from 3 to 6 different flow states when varying the position of the control rod for the same Re and geometrical parameters for the cylinder-control rod system. One of the most promising results in terms of suppressing fluctuating forces is the so-called State II reported by Cicolin et al. (2021), also called "reattachment mode" by Sakamoto and Haniu (1994), and illustrated in Fig. 2(b). Both works reported a reduction of mean drag (up to 50%) and fluctuating lift (more than 90%) relative to the cylinder in isolation for this particular flow state at moderate values of Re (2 -6×10^4). The characteristics of State II - reattachment and later separation - indicates a manifestation of the Coandă effect, in which a jet deviates its original direction to adhere to a low-pressure region of a wall, and suffers a later separation when the adverse pressure gradient reaches a critical value.

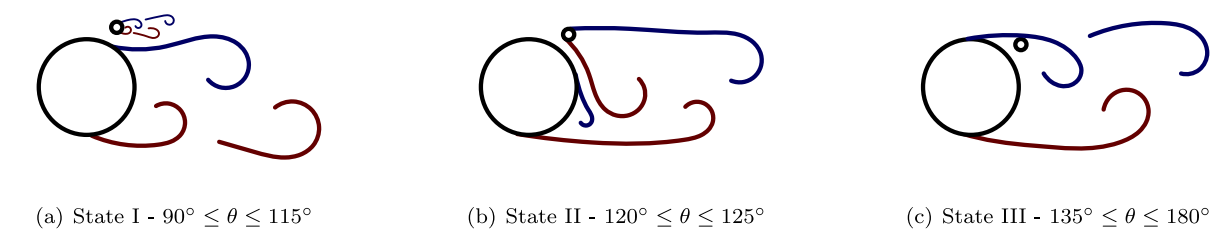


Fig. 2. Schematics for the three flow states for the cylinder with one control rod by Cicolin et al. (2021). Re = 20,000, R'/D = 0.7 and d/D = 0.1.

For example, for a rod placed at $\theta=120^\circ$, Cicolin et al. (2021) observed a separation after 180°. A pattern similar to State II was also observed by Tsutsui et al. (1997) and Kuo et al. (2007) using a control rod of a size similar to the main cylinder and different ranges of Re. According to Cicolin et al. (2021), this flow state occurs for a narrow range of rod positions between State I, characterised by two distinct wakes produced by both the cylinder and the control rod, and State III where the control rod is situated in the recirculation region of the combined system. States I and III are illustrated in Figs. 2(a) and 2(c), respectively. Note that the three flow states illustrated in Fig. 2 are produced when the angle θ of the control rod is varied whilst all other dimensionless parameters remain fixed Re=20,000, R'/D=0.7, and d/D=0.1 State II yielded the best performance in terms of suppressing the vortex shedding and reducing the mean drag force. However, this was accompanied by a significant mean lift force induced by the jet between the cylinder and control rod which broke the symmetry of the mean wake of the system. Indeed, the magnitude of the total hydrodynamic force acting on the system (lift + drag) was found to be similar to the mean drag of a cylinder in isolation (bare cylinder).

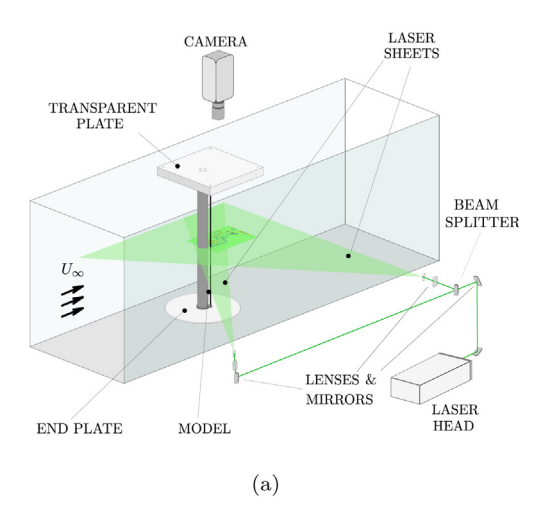
The objective of the present work is to identify whether the advantages of suppressing the fluctuating force and mean drag on the system in State II can be retained whilst mitigating against the disadvantage of a substantial mean lift force by using a symmetrical configuration of two control rods arranged in similar angular positions to that from the single-control-rod study in Cicolin et al. (2021). All other parameters (R'/D, d/D, Re) will be kept the same with the only difference being the introduction of a second control rod at location $-\theta$. Ideally, such a symmetric system geometry should produce a symmetric mean wake, eliminating the mean lift force. In short, we intend to (i) investigate if the State II flow pattern based on the Coandă effect occurs when two control rods are used; (ii) characterise the flow dynamics for the cases with two control rods; and (iii) evaluate the effectiveness of using two control rods to suppress hydrodynamic forces (both fluctuating and mean). The manuscript is structured as follows: Section 2 presents the description of the experimental setup and cases tested. Section 3.1 characterises the flow for the cylinder controlled by one rod, complementing the observations of Sakamoto and Haniu (1994) and Cicolin et al. (2021). Section 3.2 explores the dynamics of the wake for the cylinder controlled by the pair of rods in a symmetric configuration. Section 3.3 compares the one-rod and two-rods configurations, adding their effectiveness regarding their force coefficients, and Section 4 summarises the main conclusions of the work.

2. Experimental arrangement and methodology

The experiments were carried out in the recirculating water channel of the Department of Aeronautics at Imperial College London. The free-surface facility has a 0.6 m wide test section of length 8.2 m which was filled to a depth of 0.6 m. The main cylinder was an acrylic tube of diameter D=50 mm and length $L_c=540$ mm, whereas the control rod had a diameter of d = D/10 = 5 mm and the same length L_c as the main cylinder. The centre-to-centre distance between the cylinder and the control rod was R' = 0.7D = 35 mm. The coordinate system is illustrated in Fig. 1. The angular position of the control rod θ was varied between 120° and 125°, and configurations of both one- and two-rods were tested. For all experiments the flow velocity was set to $U_{\infty}=0.4$ m/s, ensuring Re=20,000, and at this speed the turbulence intensity in the water channel is approximately 1.5% at cylinder's fixed location. A thorough characterisation of the freestream turbulence in this facility, including its two-point correlation can be found in Baj and Buxton (2017). The blockage ratio was about 9% for all cases studied and was not corrected. This blockage level in water channel facilities is not expected to alter the hydrodynamic mechanisms generated by a circular cylinder significantly (Brankovic, 2006). In addition, the reference case - bare cylinder - was tested in the same conditions as were the controlled cases, minimising the influence of blockage effects on the discussion and conclusions of this paper. Two independent sets of experiments were carried out: one interrogated the flow fields using particle image velocimetry (PIV) and the other obtained the hydrodynamic forces acting on the cylinder/combined system; both sets of experiments are fully described in Section 2.1 and Section 2.2 respectively.

2.1. PIV measurements

This campaign focused on planar PIV measurements at the midspan of the cylinder, as illustrated in Fig. 3(a). The main cylinder model was attached to two acrylic plates at its extremities. In order to avoid optical distortion caused by



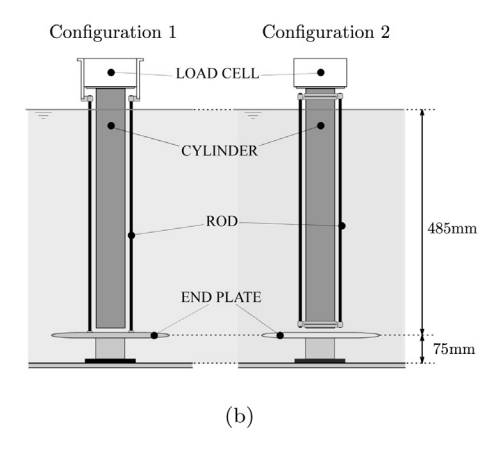


Fig. 3. (a) Arrangement of model, cameras and laser sheet in the flume for the PIV measurements and (b) Arrangement of the system for force measurements. Configuration acquiring the forces on the main cylinder only (left) and on the combined system (right).

free-surface effects, the square plate at the top was partially immersed in the water. In addition, the acrylic plate was positioned in parallel with the laser sheet and the camera. The circular plate at the bottom acted as an end plate. The gap of 50 mm from the flume's floor to the end plate isolated the cylinder from the effects of the water channel's bottom-wall boundary layer. Two support discs were responsible for connecting the cylinder and the control rod at their extremities, with a fixed gap between the two and provision to vary the control rod's angular position. For all test cases this support system maintained the control rod's rigidity with minimal hydro-elastic deflection being observed. The PIV measurements were carried out at a uniform flow velocity of 0.4 m/s. For each run, the flow was established by accelerating the flume from stationary up to the desired velocity, and the acquisition started after the stabilisation of the flow.

The illumination source was a high-speed Litron LDY304 Nd:YLF laser, which operated at a constant frequency of 800 Hz. An optical system formed by mirrors, lenses, and a 50:50 beam splitter directed the laser beam through the channel's glass walls. The laser beam was split with a 50:50 beam splitter in order to produce two separate, but coplanar, light sheets as illustrated in Fig. 3(a). The purpose of this was to ensure that the gap between the cylinder and the control rod was illuminated, and not optically inaccessible due to the shadow cast by the control rod, which turned out to be a limitation of the experiments reported in Cicolin et al. (2021). This is a particularly "active" region of the flow, with the suggestion of the presence of a separation bubble for some values of θ reported by Cicolin et al. (2021). Both light sheets were formed by a combination of one spherical and one cylindrical lens. The flow was seeded with polyamide particles with an average diameter of 7 μ m according to the manufacturer. The camera was a Phantom v641 model with maximum resolution of 2460 \times 1600 px and internal storage for 5700 images at the highest resolution. It focused on a 207 \times 114 mm Field of View (FoV), imaged via a Nikkon 60 mm f = 2.8 lens. Image pairs, offset by time delay $\Delta t = 1250~\mu$ s, were acquired at a frequency of $f_{acq} = 16$ Hz, which was synchronised to the pulsing of the laser through an external pulse generator (Stanford Research Systems DG645).

The velocity fields were computed, after the images had been pre-processed, using the commercial software *DaVis* 8.4. Initially a Gaussian filter was applied to the raw images followed by the subtraction of the mean local intensity from a 3×3 px² neighbourhood. Every pixel then had its intensity confined between a minimum of 0 and a maximum of 2000 counts. This pre-processing was performed to smooth the image, mitigate the interference of the image background, and prevent vector contamination by high-intensity peaks. Velocity fields were calculated using a standard multi-pass cross correlation method. The first step had a single pass, 50% window overlap (WO), and a 36×36 px² interrogation window (IW), whereas the second and final pass had a 12×12 px² interrogation window with a 50% overlap. Other main experimental parameters include the number of images ($N_{acq} = 3040$), time interval between adjacent images ($\Delta t = 1250\mu s$), and the final spatial resolution ($\Delta x = 0.97$ mm). As for post processing, a universal outlier detector filter (Westerweel and Scarano, 2005) with size 5×5 vector neighbourhood was applied to remove spurious vectors. For each test case, the total number of replaced vectors was lower than 1% of the total.

In order to visualise the dominant structures in the near wake more clearly, the processed velocity fields were post-processed using a "smart filtering" technique based on Optimal-Mode-Decomposition (OMD). This "smart-filtering" operation was intended to remove the fine-scale and incoherent turbulent fluctuations of the wake whilst retaining the dominant coherent structures. OMD, first proposed by Wynn et al. (2013), is a generalisation of the Dynamical Mode Decomposition (Schmid, 2010). The formulation used in this paper is the same as that described in the appendix of Cicolin et al. (2021), using an algorithm based on Wynn et al. (2013), and further discussed in Baj et al. (2015) and Rodríguez-López et al. (2016). OMD is used here mainly for visualisation purposes, when instantaneous fields are shown. One

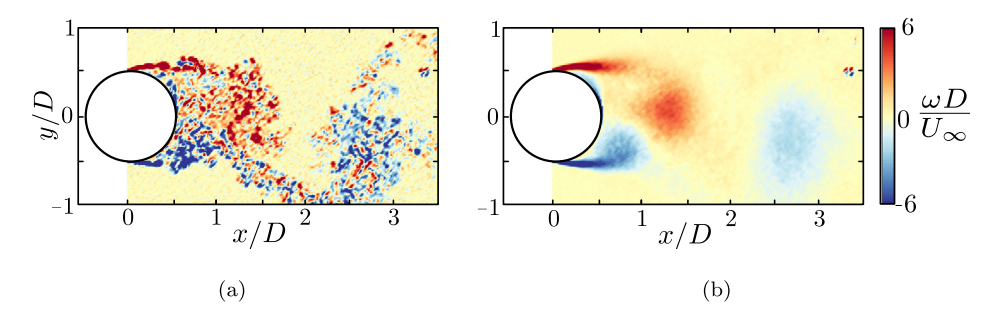


Fig. 4. Instantaneous vorticity fields (a) before and (b) after the OMD based "smart-filtering" process. Case: bare cylinder.

important exception is that the dominant OMD mode, associated with the vortex shedding, is used to provide the reference phase signal when conducting phase-averaging of the velocity/vorticity fields. The raw data was used for calculating pertinent wake quantities such as average fields, spectra, velocity at one point etc. Fig. 4 shows examples of a vorticity field reconstructed using the OMD-based "smart filter" for the bare cylinder, i.e. the main cylinder without any control rod. The filtered field on the right shows a comprehensible figure retaining the most relevant structures in the flow, the von Kármán vortex street, whereas the raw field on the left is characterised by a high-level of turbulence, as would be expected at Re = 20,000. In this paper, all the OMD-reconstructed fields used a low order model with r = 24 modes.

2.2. Force measurements

In this campaign, one extremity of the cylinder was attached to a load cell placed just above the water level. The other extremity was close to an end plate fixed to the bottom wall of the flume, intended to prevent the boundary layer effects from interfering with the flow. Fig. 3(b) shows the configuration for this campaign of experiments. The gap between the cylinder and the end plate was kept minimal by controlling the cylinder height with a jack fixed in the flume, so that the forces on the end plate were not measured by the transducer. The load cell used was an ATI Gamma IP68-SI-65-5 Force Transducer, capable of acquiring forces up to 65 N in the x- and y-directions with a resolution of ± 0.012 N. Each run was acquired at a constant rate of 200 Hz with an acquisition period of 200 s.

The experiments were carried out in two different configurations, one measuring the forces on the cylinder only (configuration 1), and another measuring the forces over the whole system, i.e. cylinders and control rods (configuration 2). This was made possible by using two different types of support to connect the control rods: one attached to the outer part of the load cell at the top and the end plate at the bottom, and the other connected directly to the main cylinder, as illustrated in Fig. 3(b). The forces of drag (F_D) and lift (F_L) for the main cylinder in configuration 1 were used for evaluating the force coefficients (C_D and C_L , respectively) for the main cylinder. For illustration, $C_D(t) = 2F_D(t)/(\rho LDU_\infty^2) = \overline{C}_D + C_D'(t)$, where \overline{C}_D is the mean, and $C_D'(t)$ the fluctuating drag coefficient in time. C_D' values shown in the results were obtained by the Root-Mean-Square (RMS) of $C_D'(t)$. The mean force on the control rods was calculated by subtracting the mean force in configuration 1 from the mean force in configuration 2 ($\overline{C}_D^{rod} = \overline{C}_D^{conf.2} - \overline{C}_D^{conf.1}$). Configuration 1 also allowed the evaluation of fluctuating force coefficients for the cylinder however, it was not possible to deduce the fluctuating forces on the control rods. For the cylinder in isolation, i.e. the cylinder without any control rod and hereafter called the bare cylinder, the value measured for the mean drag was $\overline{C}_D = 1.10$, which is in good agreement with the literature for studies at similar Reynolds number (e.g. Zdravkovich, 1997). The fluctuating lift coefficient $C_L' = 0.27$ also agrees with past research (Norberg, 2003; Khalak and Williamson, 1996). The Strouhal number was obtained through the spectrum of the lift force, as the frequency at which the spectrum peaks. The value computed was St = 0.19, also close to that measured by other researchers and compiled by Norberg (2001).

3. Results

3.1. Cylinder with one control rod

This section reports the main characteristics of the wake for a cylinder with a single control rod at the angular positions of $\theta=120^\circ$ and 125° . It reproduces the experiments of Cicolin et al. (2021) for State II but includes new, previously inaccessible information about the flow in the region between the cylinder and the control rod, made possible with the improved experimental configuration described in Section 2.1. The flow in the gap reveals important differences between the cases $\theta=120^\circ$ and 125° not previously reported in Cicolin et al. (2021).

The formation of the wake for the two values of θ are similar. Fig. 5 shows phase-averaged vorticity fields for the case $\theta = 120^{\circ}$ during one cycle of vortex shedding. Comparing it with Fig. 4(b) clarifies how the presence of the control rod modifies the wake's evolution. The top shear layer of the cylinder is diverted by the control rod, forming a strong jet that

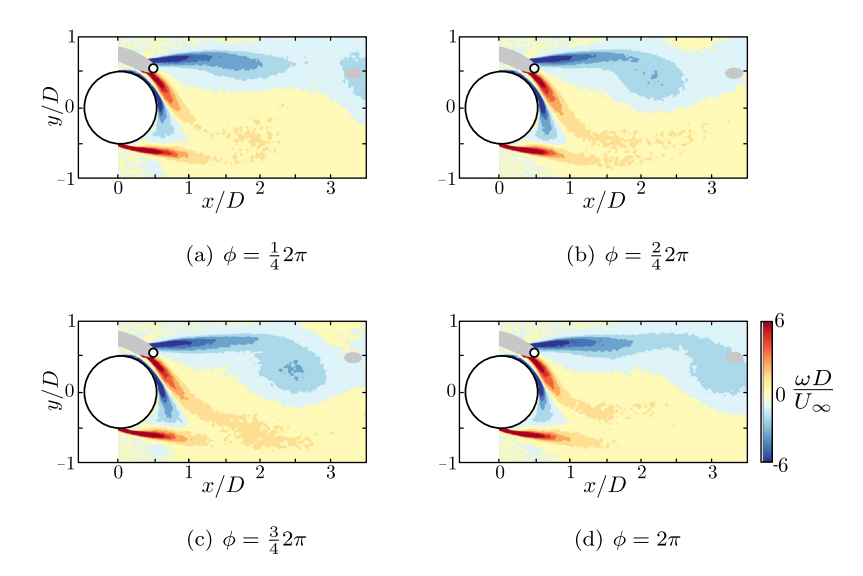


Fig. 5. Phase-averaged vorticity fields for the case $\theta = 120^{\circ}$ and one control rod.

injects momentum towards the rear face of the cylinder. Due to the Coandă effect, the boundary layer remains attached until $\theta \approx 180^\circ$, substantially farther downstream than would be expected for a bare cylinder. This delayed separation causes the short extent of the recirculation region behind the cylinder, which can be seen in Fig. 6 . The far wake of the system is the result of the interaction between the jet, the lower shear layer separating from the cylinder, and the top shear layer separating from the control rod. Further information about the wake for these configurations can be found in Cicolin et al. (2021).

Examination of the region between the cylinder and the control rod reveals that there is a small but significant difference between the cases $\theta=120^\circ$ and 125° that deserves attention. For $\theta=120^\circ$, the boundary layer remains attached until $\theta_{sep}\approx178^\circ$, as illustrated in Fig. 6(a). The separation point was identified by the PIV vector closest to the cylinder surface having zero tangential velocity. For $\theta=125^\circ$ there is a small separation bubble between 100° and 130° , which means that the boundary layer separates and reattaches to the cylinder surface before later separating permanently at $\theta_{sep}\approx182^\circ$ (Fig. 6(c)). This difference is relevant because separation bubbles are known to be a source of instability, and have been linked to bistable patterns in previous studies. Cicolin et al. (2021) observed a similar separation bubble for a bistable flow state at $\theta=130^\circ$, where the flow randomly switches from State II to State III (please refer to Fig. 2). A similar separation bubble has also been reported by Sakamoto and Haniu (1994), as one of the three quasi-stable flow states for a cylinder with one control rod at $\theta=120^\circ$ and Re=65,000. Tsutsui et al. (1997) observed a separation bubble in a stable flow for $\theta=120^\circ$ and Re=41,000, but the control rod was significantly larger ($d\approx D/3$). Here, the flow at $\theta=125^\circ$ is stable in the presence of the separation bubble, but the presence of separation bubbles will be shown to be a crucial factor in determining the stability of the flow states in the presence of two control rods explored in Section 3.2.

In comparison to the bare cylinder, the wake vortices are weaker and are shed farther downstream of the rear face of the cylinder. As a consequence, the fluctuating lift coefficient for the two controlled cases are significantly lower than for the bare cylinder: $C'_L = 0.04$ for $\theta = 120^\circ$ and $C'_L = 0.08$ for $\theta = 125^\circ$, compared to $C'_L = 0.27$ for the bare cylinder. The mean drag is also reduced due to the injection of momentum into the near wake by the jet passing between the cylinder and the control rod. The intensity of the jet can be seen in Figs. 6(b) and 6(d). $\overline{C}_D = 0.98$ for $\theta = 120^\circ$ and 0.97 for $\theta = 120^\circ$, whereas it is 1.10 for the bare cylinder. On the other hand, the jet also induces a positive mean lift on the cylinder, as $\overline{C}_L = 0.56$ for $\theta = 120^\circ$ and 0.57 for $\theta = 120^\circ$. These values are of the same order of magnitude as the drag coefficient and therefore yields a total hydrodynamic force acting on the cylinder that is similar to that for the bare cylinder; a result that is in agreement with the results of Sakamoto and Haniu (1994) and Cicolin et al. (2021). The variation between \overline{C}_D and \overline{C}_L in both cases indicates that the vector of the mean total force acts in an orientation that is more inclined towards the y-axis for the case $\theta = 125^\circ$. This is consistent with the observation from Fig. 6(c) that the angular position of the separation point θ_{sep} is further delayed for the case $\theta = 125^\circ$ relative to $\theta = 120^\circ$. A comprehensive discussion of the force coefficients, including the force on the rod and the two-rods cases, is provided in Section 3.3.

3.2. Cylinder with two, symmetrically arranged control rods

The structure of the flow for the two cases $\theta = 120^{\circ}$ and $\theta = 125^{\circ}$ is similar. Both see a jet formed between the control rods and the cylinder and delayed separation (with respect to the bare cylinder) on both sides of the cylinder. However,

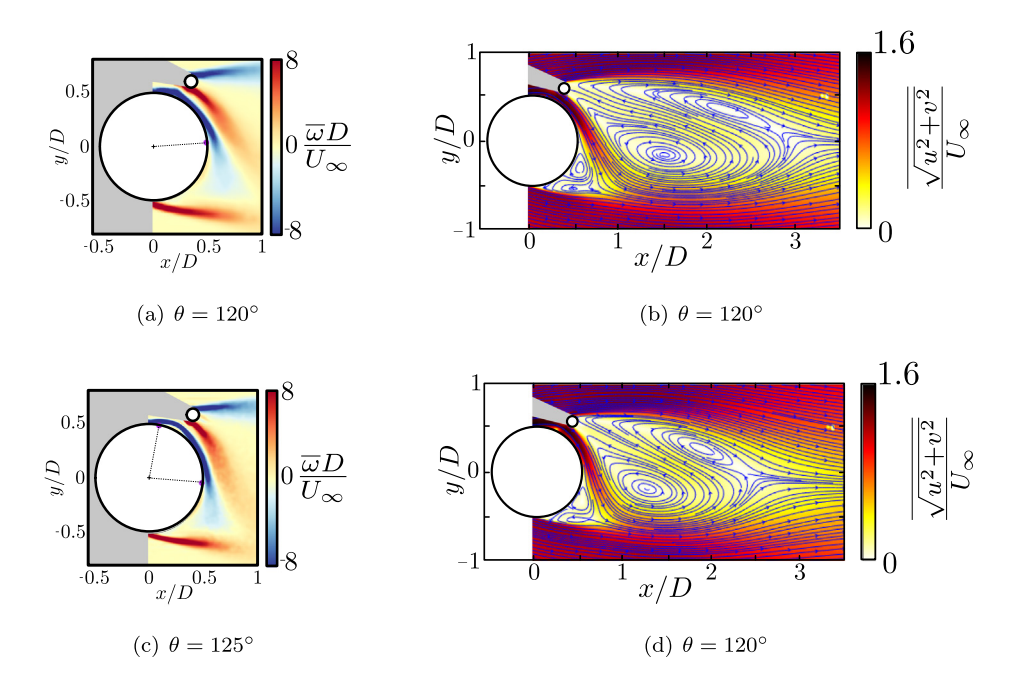


Fig. 6. Mean fields obtained from PIV for the cases with one control rod. (a-c) mean vorticity fields, where the dots in purple indicate the separation points; and (b-d) mean velocity field with streamlines. (For interpretation of the references to colour in this figure legend, the reader is referred to the web version of this article.)

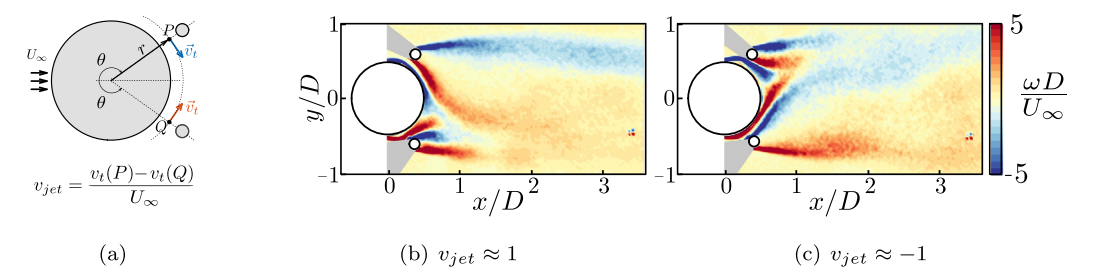


Fig. 7. Two instantaneous vorticity fields showing the two typical bistable states of the flow in State II. Case: $\theta=120^\circ$.

the flow presents bistable behaviour in both cases. At any given instant, the jet emanating from one side is stronger than the other, thereby deflecting the rear stagnation point to one side of the cylinder, i.e. a symmetric configuration yields an instantaneously asymmetric flow. Fig. 7 shows two instantaneous vorticity fields for the flow in the two different bistable states for the case $\theta = 120^{\circ}$.

In order to investigate the switching process between the two bistable states, the variable v_{jet} is introduced in Fig. 7(a). $v_{jet} = \frac{v_t(P) - v_t(Q)}{U_\infty}$ is the difference between the tangential velocities at the two mid points of the gap between the cylinder and the control rods. v_{jet} relates to the net flux of momentum into the near wake, and its orientation. Positive values indicate the wake is biased towards the bottom of the cylinder and thereby induces a positive lift, illustrated in Fig. 7(b). Contrastingly, negative values indicate that the lower jet is stronger so that the wake is biased towards the upper side, as shown in Fig. 7(c), thereby inducing a negative lift on the cylinder.

Fig. 8 shows the time series and distribution of v_{jet} for the two angular positions of the control rods tested. The two cases exhibit different behaviour regarding the average residence time spent in each bistable state. For $\theta=120^\circ$, the flow displayed different behaviour across three separate experimental runs. Each of the experimental runs was conducted after a different assembly where the positioning of the control rods was set to the same angular position of $\theta=120^\circ$ to within the experimental uncertainty which was $\pm 2^\circ$, thereby yielding slightly different configurations. In run 1, the flow switched only once, whilst it remained in the same bistable state for the entirety of the experiment in runs 2 and 3, albeit with a different bistable state in run 2 to run 3. For run 2, the wake was biased towards the top, similarly to Fig. 7(b), and for run 3 it was biased towards the bottom, similarly to 7(c). The fact that the switching was only observed once through three different runs reveals that transition from one bistable state to another is infrequent. Each run had an acquisition time greater than 300 cycles of vortex shedding for the bare cylinder (300 T_s), and the data collected is statistically insufficient to

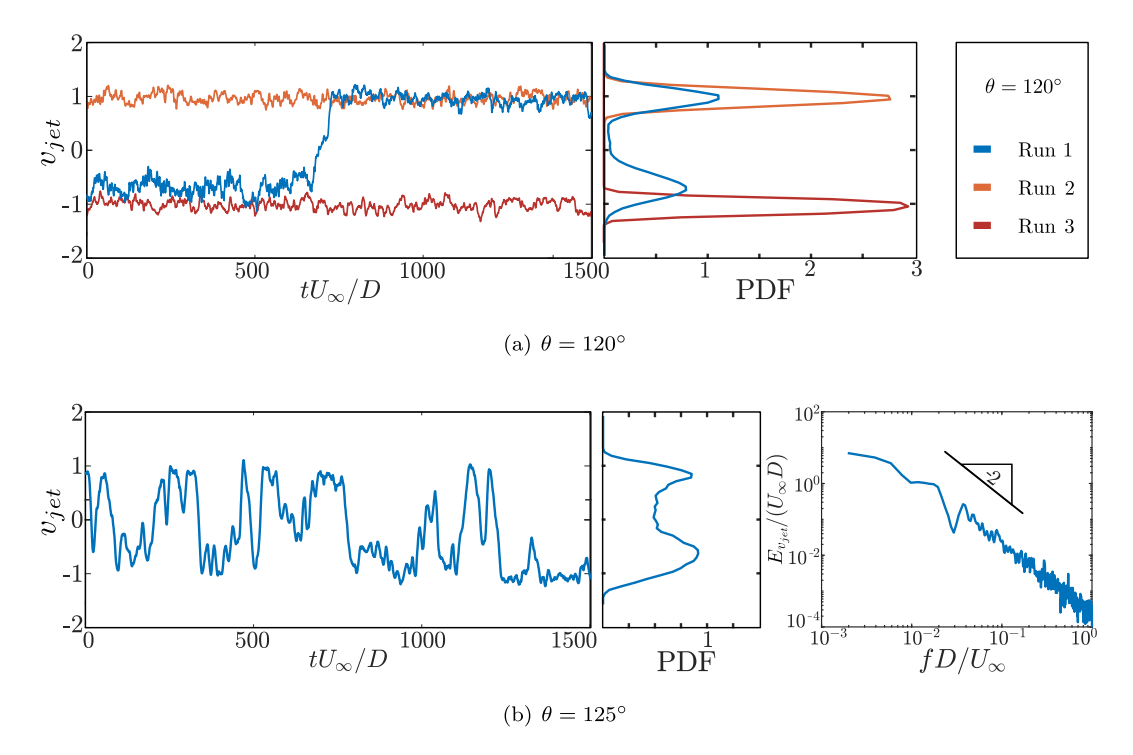
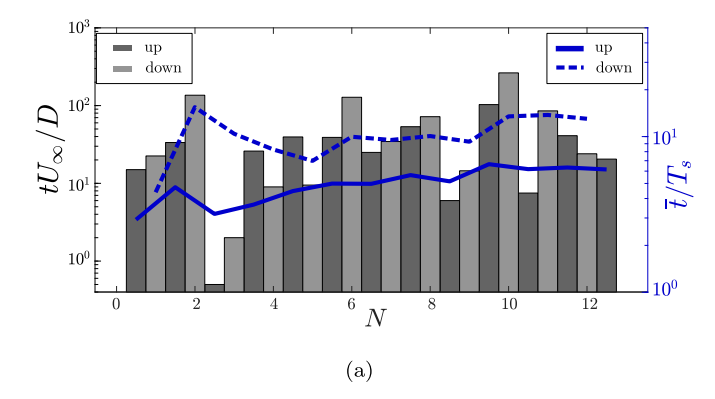


Fig. 8. Distribution of v_{jet} for the State II cases (a) Time series and Probability Density Function (PDF) for the case $\theta = 120^{\circ}$ showing three different runs. (b) Time series, PDF and spectrum of v_{jet} for the case $\theta = 125^{\circ}$.

determine its average residence time. However, the single transition observed in run 1 is important to show that the case $\theta=120^\circ$ has a bistable behaviour, and its wake asymmetry is not the mere result of the misalignment of the model. For the case $\theta=125^{\circ}$, the average residence time in each bistable state is shorter than for $\theta=120^{\circ}$, as multiple transitions were observed for a single run in Fig. 8(b). The probability density function (PDF) shows two clear peaks for viet around ± 1 , characterising the bistable behaviour. The average residence time in each state was calculated using 0 as the threshold defining switching between the two bistable states, and the result is shown in Fig. 9(a). The cumulative mean residence times, plotted in blue, converge to slight different values, which is probably a consequence of small variations in the experimental assembly, resulting in a slight misalignment (due to the previously mentioned experimental uncertainty in determining the angular position of the control rods). The average residence time in each bistable state is $\approx 10T_{\rm s}$. indicating that the bistable states have a stability period of approximately one order of magnitude longer than the vortex shedding period. However, there is not a distinct frequency associated with the switching process as can be observed in Fig. 8(b), for the spectrum has no peaks. Instead, the nature of the switching process appears to be random which can be deduced from Figs. 8 and 9(b). The spectrum of v_{iet} in the former agrees with a -2 power law at low and intermediate frequencies, which is consistent with random transitions (Grandemange, 2013). The latter plot shows, in black, a histogram of the probability that the interval between two successive transitions is greater than t/\overline{T} (where \overline{T} is the mean interval between switches) and the curve in red is $f(t) = e^{-t/\overline{T}}$. The good agreement between the black and red curves indicates that the transitions constitute a Poisson process (Mood et al., 1974).

This bistable process for the cylinder with two control rods shows some resemblance to the "flip-flopping" phenomenon present for a pair of cylinders of the same diameter put side-by-side. It was first described by Bearman and Wadcock (1973), who observed that when the spacing between the two cylinders is in a critical range then an asymmetry is introduced into the flow: there is instantaneously one wide wake with correspondingly lower *St* vortex shedding and one narrow wake with correspondingly higher *St* vortex shedding. The phenomenon has been further studied in the following decades (Williamson, 1985; Kim and Durbin, 1988; Song et al., 2015). The configuration is bistable with random switching between which cylinder produces the wide wake and which produces the narrow wake. In both the cases of the side-by-side cylinders and State II for the two-control-rods system, a symmetric configuration does not result in an instantaneously symmetric wake but a bistable behaviour of random switching between two asymmetric states (Bearman and Wadcock, 1973; Kim and Durbin, 1988). In both cases these bistabilities are very sensitive to the precise position of the assembly of cylinders/control rods.

In the search for an explanation for the distinct behaviour between the cases $\theta=120^\circ$ and 125° , it was observed that the nature of the flow separation on each side of the cylinder plays an important role. For one-control-rod, Fig. 6 shows that the boundary layer could form a separation bubble at an angular position close to that of the control rod, θ , or remain



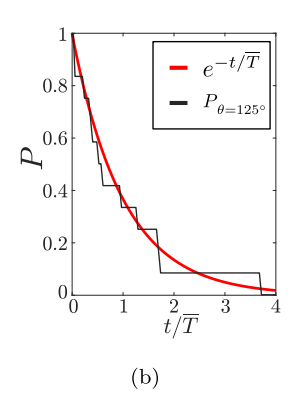


Fig. 9. (a) Residence time in the bistable states for the case $\theta = 125^{\circ}$. Up/down refers to the side towards which the wake is biased. Grey plots represent the absolute residence time in each state between transitions and blue plots represent the cumulative average. (b) Histogram of the probability of one transition to be longer than t/\overline{T} compared to the curve $e^{-t/\overline{T}}$. (For interpretation of the references to colour in this figure legend, the reader is referred to the web version of this article.)

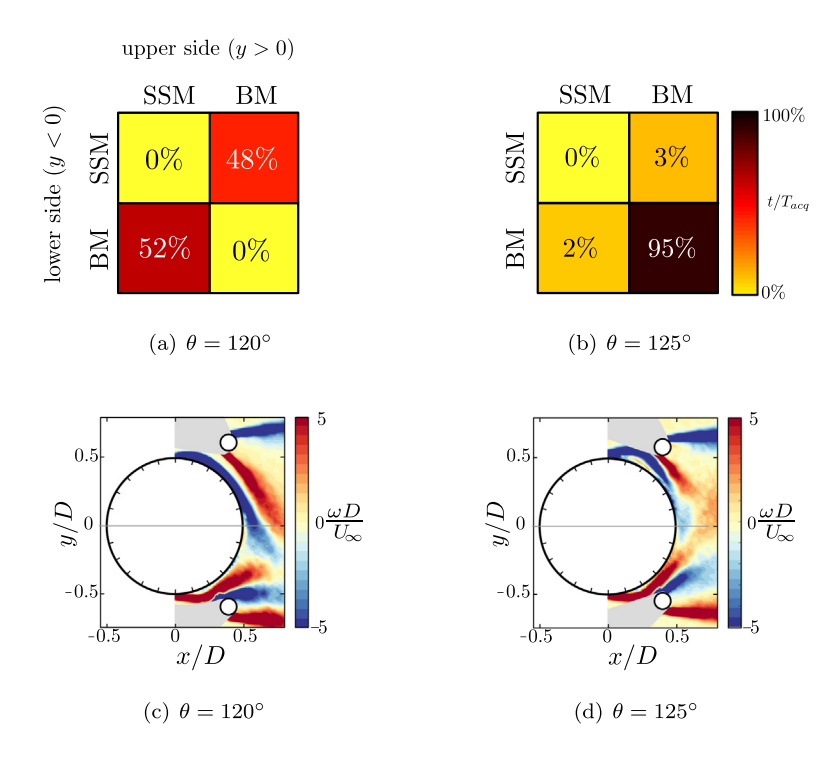
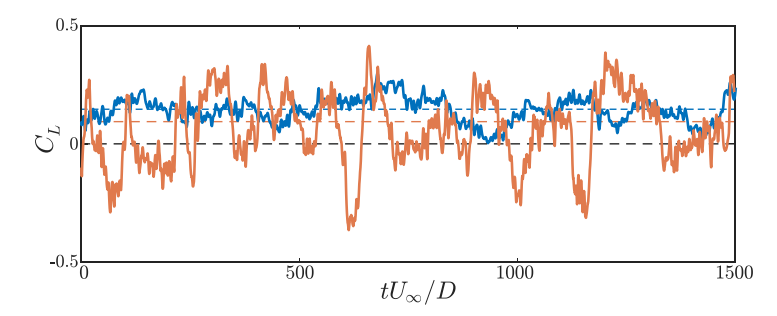


Fig. 10. Distribution of the separation types on the two sides of the cylinder (top) and instantaneous vorticity fields of the dominant flow pattern (bottom) (a)–(c) $\theta = 120^{\circ}$ and (b)–(d) $\theta = 125^{\circ}$.

attached until \approx 180°. For clarity, these two types of separation are referred to here as "single separation" mode (SSM) and "bubble" mode (BM). The identification was possible by probing the tangential velocity (v_t) close to the cylinder's surface, at a position r=0.53D. This particular position rests within the separation bubble, yielding a very low value when BM occurs ($v_t \approx 0$). If there is no separation bubble, the tangential velocity is higher, so a threshold of $v_t \geq 0.5$ was used to identify SSM.

Fig. 10 shows the combination of the separation types occurring at the two sides of the cylinder for both control-rod positions. The upper side (y > 0) is represented on the horizontal axis, whereas the lower side (y < 0) is represented on the vertical axis. The value displayed in each cell represents the time spent in each combination as a percentage of the total acquired time (T_{acq}). For the case $\theta = 120^{\circ}$, the figure shows that the cylinder only experiences separation with a bubble on one side whereas the other side experiences single separation, as illustrated in Fig. 10(c). For the case $\theta = 125^{\circ}$, the dominant combination is two separations bubbles (with subsequent reattachment) occurring simultaneously at each side of the cylinder. Separation without a bubble on both sides was never observed for either $\theta = 120^{\circ}$ or $\theta = 125^{\circ}$. These



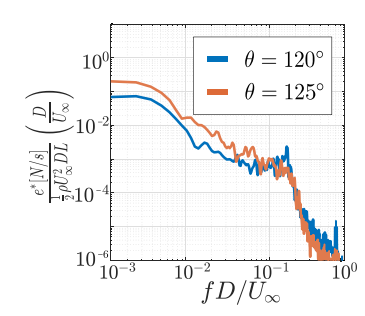


Fig. 11. Comparison between the lift force of the cases $\theta = 120^{\circ}$ and $\theta = 125^{\circ}$ with two control rods. Time series (left), where the dashed lines represent the average value for each case, and their respective spectra (right).

results, combined with the frequency of transitions between bistable states observed for the cases $\theta=120^\circ$ and $\theta=125^\circ$, indicate that the pair single-separation-and-bubble (dominant for $\theta=120^\circ$) is more stable in time than two-bubbles, as most of the transitions were observed when the flow yielded two separation bubbles, i.e. for $\theta=125^\circ$ (see Fig. 8). This is not unexpected at first, since the jet on the side without the separation bubble is stronger and much more probable to prevail against the jet emanating from the other side of the cylinder with a separation bubble. When the separation bubble occurs on both sides, the difference between the jets' intensities fluctuates more, manifesting as a more chaotic signal of v_{jet} , thereby reducing the residence period for each bistable state. In other words, the formation of a separation bubble induces more fluctuations in the gap flow than a shear layer that remains completely attached to the cylinder.

Summarising, we postulate that the imbalance between the jets emanating from the two sides of the cylinder is the key factor behind the flow's bistability/asymmetry. One could argue that the Coandă effect, a known source of instability, is the main cause of the bistability. However, the work of Chauhan et al. (2019) presents an asymmetric flow for a square cylinder manipulated with two control rods. Given the fixed-separation points of the square cylinder, the Coandă effect does not occur yet the resultant wake is asymmetric with two jets of different intensities.

Regarding the fluid forces, the mean drag acting on the cylinder was significantly reduced compared to the bare cylinder. $\overline{C}_D = 0.85$ for $\theta = 120^\circ$ and 0.78 for $\theta = 125^\circ$, which represents a reduction of 25% and 30%. A possible explanation for these large drag reductions with two control rods resides in the injection of momentum into the near wake by the two jets, driven by the low pressure in the near wake. It is consistent with the observations that both layers reattach over the cylinder, leading to a later separation due to the Coandă effect. This feature of the two-control-rod cases is different from the one-control-rod cases. In the latter, the jet emanating from one side causes the shear layer on the other side to separate earlier, creating a recirculation region dislocated from the centreline and inducing a large lift coefficient.

The mean lift is non-zero for both cases, as a consequence of the bistability and the finite sampling period, yet it is significantly lower than for the one-control-rod cases. Fig. 11 shows the time series for the two cases with their respective spectra. From the time series it is clear that the case $\theta=125^\circ$ yields larger instantaneous values of lift than $\theta=120^\circ$, and its mean lift coefficient is lower than for $\theta=125^\circ$ only because it includes multiple bistable transitions, whereas the case $\theta=120^\circ$ resided in the same bistable state for the entire acquisition period. This also provides an explanation for the lower fluctuating lift of the case $\theta=120^\circ$, $C_L'=0.05$ against $C_L'=0.12$ for $\theta=125^\circ$. Even with the bistability, the fluctuating lift for $\theta=125^\circ$ is approximately 60% lower than for the bare cylinder. The spectra on the right show that most of the energy is concentrated at low frequencies, but for the case $\theta=120^\circ$, there is a peak at around $fD/U_\infty\approx0.16$, which is associated with a vortex shedding mechanism formed downstream in the wake. The residence period in each bistable state is long enough to allow for the von Kármán vortices to shed regularly. No such peak is observed in the spectrum for the case $\theta=125^\circ$.

Fig. 12 shows a complete cycle of vortex shedding phase-averaged at the vortex-shedding frequency of $fD/U_\infty \approx 0.16$, obtained from a PIV time-series where the wake was biased towards the bottom bistable state during the whole period. It shows the formation of a vortex street after $x/D \approx 2.5$, similar to that observed for the one-control-rod State II (refer to Fig. 5), despite the clear differences in the very near wake of the main cylinder. The vortex-shedding frequency is also close to the value observed for one-control-rod (Cicolin et al., 2021).

3.3. Force measurements

This section summarises the force measurements and compares the effectiveness, from an applications standpoint, of all cases at suppressing the hydrodynamic forces. In order to facilitate the comparison, Table 1 shows the numerical values for the force coefficients. Notice that the total force magnitude was measured as the average of the instantaneous force magnitude over the combined system, i.e $\overline{C}_T = \overline{C_T(t)}$, where $C_T(t) = \sqrt{C_D(t)^2 + C_L(t)^2}$ measured in configuration 2 (Fig. 3(b)).

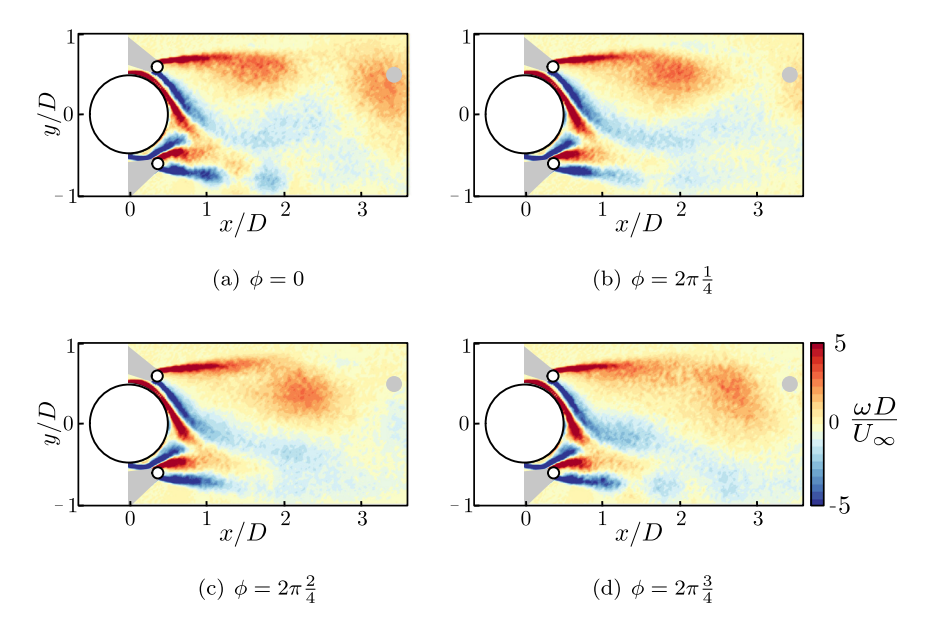


Fig. 12. Vortex shedding cycle for the case $\theta = 120^{\circ}$ with two control rods. Re = 20,000.

Table 1 Summary for the force coefficients. \overline{C}_T is the total force magnitude measured over the combined system, i.e, cylinder + rods. When considering two-control-rod cases \overline{C}_D^{rods} is the combined drag over both control rods.

	\overline{C}_D	C'_D	\overline{C}_L	C'_L	\overline{C}_D^{rods*}	\overline{C}_T
Bare cylinder	1.10	0.053	0	0.277	-	1.10
$\theta = 120^{\circ} - 1 \text{ rod}$	0.98	0.024	0.57	0.04	0.03	1.18
$\theta = 125^{\circ} - 1 \text{ rod}$	0.97	0.022	0.58	0.08	0.02	1.15
$\theta = 120^{\circ} - 2 \text{ rod}$	0.85	0.017	0.16	0.05	0.19	1.04
$\theta = 125^{\circ} - 2 \text{ rod}$	0.78	0.033	0.11	0.13	0.16	0.94

For one-control-rod, the mean drag reduction was accompanied by a surge in the mean lift, so that the total force magnitude ($\overline{C}_T = 1.17$ for $\theta = 120^\circ$ and $\overline{C}_T = 1.14$ for $\theta = 125^\circ$) was close to the value measured for the bare cylinder (1.10). These values agree with those observed by Sakamoto and Haniu (1994). Despite their not measuring the force acting on the rod this should not significantly alter their obtained value for \overline{C}_T since our results show that it accounts for less than 3% of the total force magnitude.

Adding the second control rod reduced the mean drag to a much greater extent than when compared to one-control-rod cases and the bare cylinder, and also significantly reduced the mean lift. Accordingly, the total force magnitude was significantly reduced. These results highlight that using two control rods is a more effective passive flow-control strategy than using one control rod. $\overline{C}_T = 1.04$ for $\theta = 120^\circ$ and $\overline{C}_T = 0.94$ for $\theta = 125^\circ$, which represents a drop of 6% and 15% in comparison to the bare cylinder, respectively. In contrast to the cases with only one control rod, the total force magnitude coefficient is not significantly different from the mean drag, due to the lower values of the mean lift coefficient.

comparison to the bare cylinder, respectively. In contrast to the cases with only one control rod, the total force magnitude coefficient is not significantly different from the mean drag, due to the lower values of the mean lift coefficient. There is interesting behaviour for the mean drag over the control rods (\overline{C}_D^{rods}). It is very low for the one-control-rod cases. $\overline{C}_D^{1rod} = 0.03$ for $\theta = 120^\circ$ and $\overline{C}_D^{1rod} = 0.02$ for $\theta = 125^\circ$. These are more than 70% lower than the expected value for a bare cylinder of the same dimension (i.e. with a diameter of d) and for the same incoming velocity U_∞ ($\overline{C}_D^d \approx 0.11$). Note that the incoming velocity at the location of the control rod is approximately 20%–30% higher than U_∞ , which can be estimated from Fig. 6, and so the expected drag coefficient (using U_∞ as the reference velocity scale) could be expected to be, perhaps, 50% higher still putting the extremely low values for \overline{C}_D^{1rod} into even greater perspective. \overline{C}_D^{1rod} is also lower for $\theta = 125^\circ$ than 120°, which is possibly linked to the lower incoming velocity at the control rod's position in this case, and also the presence of the separation bubble. For two-control-rod cases, however, \overline{C}_D^{2rods} is much higher than for one-control-rod: $\overline{C}_D^{2rods} = 0.19$ for $\theta = 120^\circ$ and $\overline{C}_D^{2rods} = 0.16$ for $\theta = 125^\circ$. We must point out that it comprises the sum of the two control rods, since no direct measurements could be made for each individual control rod. Regardless, the overall drag coefficient for two-control-rods is substantially more than twice that of the cases with one-control-rod. Fig. 7 shows one of the two control rods produces a much wider wake than the other. By comparing Figs. 7 and 6 we can see that the wider wake produced by one of the control rods in the two-control-rod configuration is comparable in width to that produced when only one control rod is used. Let us therefore assume that the drag produced by the control

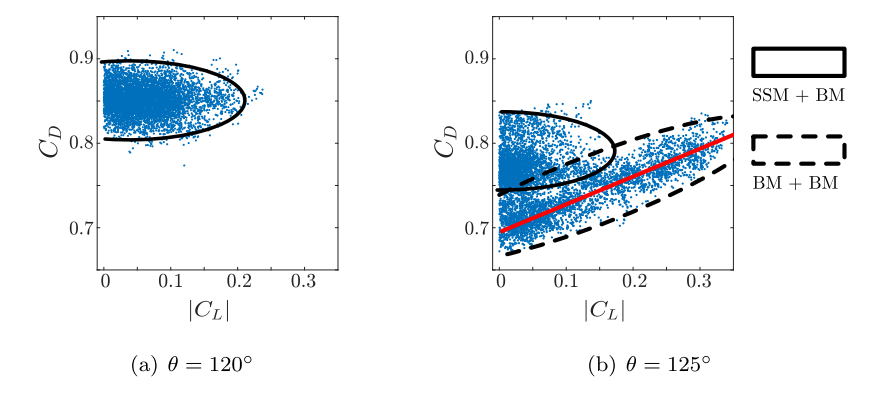


Fig. 13. C_D versus $|C_L|$ on the main cylinder for the cases (a) $\theta = 120^\circ$ and (b) 125°. The region delimited by the solid black line refer to cases where the system develops SSM on one side and BM on the other, whereas the region inside the dashed line refer to the separation type BM occurring on both sides. (For interpretation of the references to colour in this figure legend, the reader is referred to the web version of this article.)

rod with the wide wake in the two-control-rod configuration is comparable to the drag produced by the control rod in the one-control-rod configuration. If this is the case then our results indicate that the control rod with the narrow wake must produce a drag that is two to three times larger.

This result raises an interesting consequence for future applications. Consider, hypothetically, a system where the two control rods are connected to each other, with a fixed distance, but free to orbit around the centre of the main cylinder. When the bistability affects a deflection of the wake towards one particular side, the control rod suffering the higher drag would tend to move towards the centreline, pushing the other control rod to a region exposed to higher velocities, and therefore subjected to a higher drag. They would eventually reach an equilibrium that could potentially annihilate the lift force fluctuation, which is one of the most disadvantageous effect of the bistability. In addition, the drag force can be substantially reduced when the absolute lift force is eliminated. In figure we present scatter plots of instantaneous C_D versus $|C_I|$ for the cases controlled by two control rods. The regions delimited by each separation types were determined based on Fig. 10, although the data was obtained from a different experiment. Considering that $\theta = 120^{\circ}$ produced SSM+BM only, we associated the group of points in Fig. 13(a) to this type of separation. For $\theta = 125^{\circ}$, there are two main regions: one linked to the wake formed by the separation SSM on one side and BM on the other; and the wake formed by two BM. In the former, C_D is practically independent of $|C_L|$ variation, similarly to the graph for $\theta = 120^\circ$ (Fig. 13(a)). For the other region, however, there is a seemingly linear relationship between C_D and $|C_L|$ for the instants where both sides have a separation bubble. This is the region delimited by the dashed black line and red regression line in Fig. 13(b). If C_L is reduced, C_D also tends to reach a minimum. The regression line in red shows that the mean drag coefficient can reach values as low as 0.68, almost 40% lower than the mean drag coefficient for the bare cylinder. It indicates that this type of control has a greater potential for drag reduction, which deserves further attention in future research.

4. Conclusions

Experiments were carried out with a circular cylinder at Re = 20,000 manipulated by one or two control rods with diameters ten times smaller than the cylinder itself, placed at a centre-to-centre distance of R'/D = 0.7 and at angular positions of $\theta = 120^{\circ}$ or 125° . The results were presented in terms of PIV velocity fields and force measurements. When a single control rod was placed in the same $(R'/d, \theta)$ positions at this Reynolds number a State II flow, as characterised by Cicolin et al. (2021), was produced. Of the three flow states identified by Cicolin et al. (2021) State II showed the greatest promise in terms of reducing the drag, and fluctuating forces, acting on the cylinder. The major drawback of the single-control-rod configuration was that it induced a large mean lift meaning that the mean overall hydrodynamic force acting on the combined cylinder plus control-rod system was greater than the mean drag on the bare cylinder. The primary objective of our work was therefore to mitigate against this shortcoming of State II flows by introducing a second control rod such that the two control rods were placed at $\pm \theta$ to induce a symmetric configuration and thereby try to force a symmetric flow with zero mean lift. In particular, we investigated if the same flow state (State II), characterised by a late separation induced by the Coandă effect, occurs for the system with two control rods. Subsequently, we characterised the dynamics of the flow in this two-control-rod configuration and finally analysed its effectiveness at suppressing the hydrodynamic forces. Additionally, with an improved experimental set up we sought to examine the flow in the region between the cylinder and the control rod in the one-control-rod configuration since this is a particularly active region of the flow and the results of Cicolin et al. (2021) hinted at the possibility of a separation bubble forming here.

For one-control-rod, the wake is characterised by a strong jet between the cylinder and the control rod, a small recirculation region downstream of the cylinder and deflected downwards, and a large recirculation region downstream of the rod. The main difference between the cases $\theta = 120^{\circ}$ and $\theta = 125^{\circ}$ was that the boundary layer separates and

reattaches to the cylinder's surface for $\theta=125^\circ$, forming a small separation bubble, and remains attached until $\theta_{sep}\approx180^\circ$ for $\theta=120^\circ$.

When the second control rod was introduced we confirmed that a flow state characterised by jets passing between the control rods and the cylinder, and delayed separation from the rear face of the cylinder induced by the Coandă effect exists, i.e. a flow state that is extremely similar to State II for the one-control-rod configuration.

However, the wake develops a bistable behaviour induced by the imbalance of the two jets, emanating from the gap between the cylinder and the control rods, which collide with one another close to the rear face of the cylinder. The phenomenology of this bistability is random with a characteristic time of transitioning between the two bistable states several times longer than the regular vortex-shedding period. The residence time in each bistable state is also strongly dependent on the exact position of the control rods. The nature of the flow's separation, with or without a separation bubble close to the position of the control rods and subsequent reattachment, played a decisive role in determining the dynamics of the bistability. It was shown that the system is more susceptible to switch when a separation bubble is present on both sides.

Regarding the fluid forces, all of the cases tested are effective at reducing the mean drag and fluctuating lift acting on the cylinder. However, for the cases with one-control-rod, there is a large mean lift coefficient that yields a total mean force magnitude greater than the mean drag of the bare cylinder. For two-control-rods, however, the total force magnitude is reduced relative to the mean drag of the bare cylinder. The overall reduction, considering cylinder and control rods together, is of 8% for $\theta=120^\circ$ and 16% for $\theta=125^\circ$. Looking carefully at the behaviour of the forces over the control rods and the cylinder, it is suggested that the possibility exists for the drag force on the main cylinder to be reduced by up to 40% if the mean lift is suppressed, i.e, if the bistability is controlled, leading to a drag reduction of up to 30% for the total system.

Declaration of competing interest

The authors declare that they have no known competing financial interests or personal relationships that could have appeared to influence the work reported in this paper.

Data availability

Data will be made available on request

Acknowledgements

We gratefully acknowledge support of the RCGI Research Centre for Gas Innovation, hosted by the University of São Paulo and sponsored by FAPESP São Paulo Research Foundation, Brazil (2014/50279-4) and Shell Brasil, and the support of ANP Brazil's National Oil, Natural Gas and Biofuels Agency through the R&D levy regulation. M.M.Cicolin is thankful for the support of CNPq, Brazil (201176/2018-1).

References

- Assi, G., Orselli, R., Silva-Ortega, M., 2019. Control of vortex shedding from a circular cylinder surrounded by eight rotating wake-control cylinders at Re = 100. J. Fluids Struct. 89, 13–24. http://dx.doi.org/10.1016/j.jfluidstructs.2019.03.003, URL https://www.sciencedirect.com/science/article/pii/S0889974618307825. Bluff Body Wakes and Vortex-induced Vibrations (BBVIV-7).
- Baj, P., Bruce, P., Buxton, O., 2015. The triple decomposition of a fluctuating velocity field in a multiscale flow. Phys. Fluids 27, 075104. http://dx.doi.org/10.1063/1.4923744.
- Baj, P., Buxton, O., 2017. Interscale energy transfer in the merger of wakes of a multiscale array of rectangular cylinders. Phys. Rev. Fluids 2, http://dx.doi.org/10.1103/PhysRevFluids.2.114607.
- Bearman, P.W., 1984. Vortex Shedding from oscillating Bluff Bodies. Annu. Rev. Fluid Mech. 16, 195–222. http://dx.doi.org/10.1146/annurev.fl.16. 010184.001211.
- Bearman, P.W., Wadcock, A.J., 1973. The interaction between a pair of circular cylinders normal to a stream. J. Fluid Mech. 61 (3), 499–511. http://dx.doi.org/10.1017/S0022112073000832.
- Bingham, C., Morton, C., Martinuzzi, R., 2018. Influence of control cylinder placement on vortex shedding from a circular cylinder. Exp. Fluids 59, 158. http://dx.doi.org/10.1007/s00348-018-2615-z.
- Blevins, R., 2001. Flow-Induced Vibration. Krieger Publishing Company, URL https://books.google.co.uk/books?id=Wzo8PgAACAAJ.
- Brankovic, M., 2006. Vortex-Induced vibration attenuation of circular cylinders with low mass and damping (Ph.D. thesis). Imperial College London. Chauhan, M.K., Dutta, S., Gandhi, B.K., 2019. Wake flow modification behind a square cylinder using control rods. J. Wind Eng. Ind. Aerodyn. 184, 342–361. http://dx.doi.org/10.1016/j.jweia.2018.12.002, URL https://www.sciencedirect.com/science/article/pii/S0167610518305993.
- Choi, H., Jeon, W., Kim, J., 2008. Control of flow over a bluff body. Annu. Rev. Fluid Mech. 40, 131–139. http://dx.doi.org/10.1146/annurev.fluid.39. 050905.110149.
- Cicolin, M., Buxton, O., Assi, G., Bearman, P., 2021. The role of separation on the forces acting on a circular cylinder with a control rod. J. Fluid Mech. 915, A33. http://dx.doi.org/10.1017/jfm.2021.64.
- Dalton, C., Xu, Y., Owen, J., 2001. The suppression of lift on a circular cylinder due to vortex shedding at moderate Reynolds numbers. J. Fluids Struct. 15, 617–628. http://dx.doi.org/10.1006/jfls.2000.0361.
- Faltinsen, O., 1990. Sea Loads on Ships and Offshore Structures. Cambridge University Press.
- Grandemange, M., 2013. Analysis and control of three-dimensional turbulent wakes: from axismmetric bodies to road vehicles (Ph.D. thesis). ENSTA ParisTech.

- Jimenez-Gonzalez, J., Huera-Huarte, F., 2017. Experimental sensitivity of vortex-induced vibrations to localized wake perturbations. J. Fluids Struct. 74, 53–63. http://dx.doi.org/10.1016/j.jfluidstructs.2017.07.010.
- Jiménez-González, J., Huera-Huarte, F., 2018. Vortex-induced vibrations of a circular cylinder with a pair of control rods of varying size. J. Sound Vib. 431, 163–176. http://dx.doi.org/10.1016/j.jsv.2018.06.002, URL http://www.sciencedirect.com/science/article/pii/S0022460X18303560.
- Khalak, A., Williamson, C.H.K., 1996. Dynamics of a hydroelastic cylinder with very low mass and damping. J. Fluids Struct. 10 (5), 455-472. http://dx.doi.org/10.1006/jfls.1996.0031, URL http://www.sciencedirect.com/science/article/pii/S0889974696900316.
- Kim, H.J., Durbin, P.A., 1988. Investigation of the flow between a pair of circular cylinders in the flopping regime. J. Fluid Mech. 196, 431–448. http://dx.doi.org/10.1017/S0022112088002769.
- Kuo, C.-H., Chiou, L.-C., Chen, C.-C., 2007. Wake flow pattern modified by small control cylinders at low Reynolds number. J. Fluids Struct. 23 (6), 938–956. http://dx.doi.org/10.1016/j.jfluidstructs.2007.01.002, URL http://www.sciencedirect.com/science/article/pii/S0889974607000114.
- Mittal, S., Raghuvanshi, A., 2001. Control of vortex shedding behind circular cylinder for flows at low Reynolds numbers. Internat. J. Numer. Methods Fluids 35, 421–447. http://dx.doi.org/10.1002/1097-0363(20010228)35:4<421::AID-FLD100>3.0.CO;2-M.
- Mood, A.M., Franklin, A., Boes, D.C., 1974. Introduction To the Theory of Statistics. In: Oxford Science Publications, McGraw-Hill.
- Norberg, C., 2001. Flow around a circular cylinder: Aspects of the fluctuating lift. J. Fluids Struct. 15 (3), 459–469. http://dx.doi.org/10.1006/jfls.2000. 0367, URL http://www.sciencedirect.com/science/article/pii/S0889974600903670.
- Norberg, C., 2003. Fluctuating lift on a circular cylinder: review and new measurements. J. Fluids Struct. 17 (1), 57–96. http://dx.doi.org/10.1016/S0889-9746(02)00099-3, URL http://www.sciencedirect.com/science/article/pii/S0889974602000993.
- Païdoussis, M.P., Price, S.J., de Langre, E., 2010. Fluid-structure interactions: Cross-flow-induced instabilities. Cambridge University Press, http://dx.doi.org/10.1017/CB09780511760792.
- Parezanovic, V., Cadot, O., 2012. Experimental sensitivity analysis of the global properties of a two-dimensional turbulent wake. J. Fluid Mech. 693, 115–149. http://dx.doi.org/10.1017/jfm.2011.495.
- Parezanovic, V., Monchaux, R., Cadot, O., 2015. Characterization of the turbulent bistable flow regime of a 2D bluff body wake disturbed by a small control cylinder. Exp. Fluids 56–12, 1–8. http://dx.doi.org/10.1007/s00348-014-1890-6.
- Rodríguez-López, E., Bruce, P.J.K., Buxton, O.R.H., 2016. Near field development of artificially generated high Reynolds number turbulent boundary layers. Phys. Rev. Fluids 1, 074401. http://dx.doi.org/10.1103/PhysRevFluids.1.074401, URL https://link.aps.org/doi/10.1103/PhysRevFluids.1.074401. Sakamoto, H., Haniu, H., 1994. Optimum suppression of fluid forces acting on a circular cylinder. J. Fluids Eng. 116, 221–227. http://dx.doi.org/10. 1115/1.2910258.
- Sakamoto, H., Tan, K., Haniu, H., 1991. An optimum suppression of fluid forces by controlling a shear layer separated from a square prism. J. Fluids Eng. 113, 183–189. http://dx.doi.org/10.1115/1.2909478.
- Schmid, P., 2010. Dynamic mode decomposition of numerical and experimental data. J. Fluid Mech. 656, 5-28. http://dx.doi.org/10.1017/ S0022112010001217.
- Song, F.-L., Tseng, S.-Y., Hsu, S.-W., Kuo, C.-H., 2015. Gap ratio effect on flow characteristics behind side-by-side cylinders of diameter ratio two. Exp. Therm Fluid Sci. 66, 254–268. http://dx.doi.org/10.1016/j.expthermflusci.2015.04.001.
- Strykowski, P., Sreenivasan, R., 1990. On the formation and suppression of vortex 'shedding' at low Reynolds numbers. J. Fluid Mech. 218, 71–107. http://dx.doi.org/10.1017/S0022112090000933.
- Tsutsui, T., Igarashi, T., Kamemoto, K., 1997. Interactive flow around two circular cylinders of different diameters at close proximity. Experiment and numerical analysis by vortex method. J. Wind Eng. Ind. Aerodyn. 69–71, 279–291. http://dx.doi.org/10.1016/S0167-6105(97)00161-X.
- Westerweel, J., Scarano, F., 2005. Universal outlier detection for PIV data. Exp. Fluids 39, 1096–1100. http://dx.doi.org/10.1007/s00348-005-0016-6. Williamson, C.H.K., 1985. Evolution of a single wake behind a pair of bluff bodies. J. Fluid Mech. 159, 1–18. http://dx.doi.org/10.1017/
- Williamson, C.H.K., 1996. Vortex dynamics in the cylinder wake. Annu. Rev. Fluid Mech. 28, 477–539. http://dx.doi.org/10.1146/annurev.fl.28.010196. 002401.
- Williamson, C., Govardhan, R., 2004. Vortex-induced vibrations. Annu. Rev. Fluid Mech. 36 (1), 413–455. http://dx.doi.org/10.1146/annurev.fluid.36. 050802.122128.
- Wynn, A., Pearson, D., Ganapathisubramani, B., Goulart, P., 2013. Optimal mode decomposition for unsteady flows. J. Fluid Mech. 733, 473–503. http://dx.doi.org/10.1017/jfm.2013.426.
- Yildirim, I., Rindt, C.C.M., Steenhoven, A.A., 2010. Vortex dynamics in a wire-disturbed cylinder wake. Phys. Fluids 22, 094101. http://dx.doi.org/10. 1063/1.3466659.
- Zdravkovich, M., 1981. Review and classification of various aerodynamic and hydrodynamic means for suppressing vortex shedding. J. Wind Eng. Ind. Aerodyn. 7 (2), 145–189. http://dx.doi.org/10.1016/0167-6105(81)90036-2, URL http://www.sciencedirect.com/science/article/pii/0167610581900362.
- Zdravkovich, M., 1997. Flow around circular cylinders. In: Fundamentals. Vol. I, Oxford Science Publications.
- Zhu, H., Yao, J., Ma, Y., Zhao, H., Tang, Y., 2015. Simultaneous CFD evaluation of VIV suppression using smaller control cylinders. J. Fluids Struct. 57, 66–80. http://dx.doi.org/10.1016/j.jfluidstructs.2015.05.011.